

1 **Acute respiratory infection in human dipeptidyl peptidase 4-transgenic**  
2 **mice infected with Middle East respiratory syndrome coronavirus**

3

4 Naoko Iwata-Yoshikawa,<sup>a†</sup> Tadashi Okamura,<sup>a,b,c†</sup> Yukiko Shimizu,<sup>b</sup> Osamu Kotani,<sup>d</sup>  
5 Hironori Sato,<sup>d</sup> Hanako Sekimukai,<sup>a,e</sup> Shuetsu Fukushi,<sup>f</sup> Tadaki Suzuki,<sup>a</sup> Yuko Sato,<sup>a</sup>  
6 Makoto Takeda,<sup>g</sup> Masato Tashiro,<sup>h</sup> Hideki Hasegawa,<sup>a</sup> and Noriyo Nagata<sup>a#</sup>

7 <sup>a</sup>Department of Pathology, National Institute of Infectious Diseases, Tokyo, Japan;

8 <sup>b</sup>Department of Laboratory Animal Medicine, Research Institute, National Center for

9 Global Health and Medicine (NCGM), Tokyo, Japan; <sup>c</sup>Section of Animal Models,

10 Department of Infectious Diseases, Research Institute National Center for Global Health

11 and Medicine, Tokyo, Japan; <sup>d</sup>Laboratory of Viral Genomics, Pathogen Genomics Center,

12 National Institute of Infectious Diseases, Tokyo, Japan; <sup>e</sup>Department of Tissue Physiology,

13 Faculty of Agriculture, Tokyo University of Agriculture and Technology, Tokyo, Japan;

14 <sup>f</sup>Department of Virology I, National Institute of Infectious Diseases, Tokyo, Japan;

15 <sup>g</sup>Department of Virology III, National Institute of Infectious Diseases, Tokyo, Japan;

16 <sup>h</sup>Influenza Virus Research Center, National Institute of Infectious Diseases, Tokyo, Japan

17 Running head: A transgenic mouse model of MERS-CoV

18

19 #Address correspondence to Noriyo Nagata, nnagata@niid.go.jp.

20 †N.I.-Y. and T.O. contributed equally to this work.

21

22 Word counts: abstract, 216 words

23

24 **ABSTRACT**

25 Middle East respiratory syndrome coronavirus (MERS-CoV) infection can manifest  
26 as a mild illness, acute respiratory distress, organ failure, or death. Several animal models  
27 have been established to study disease pathogenesis and to develop vaccines and  
28 therapeutic agents. Here, we developed transgenic (Tg) mice on a C57BL/6 background;  
29 these mice expressed human CD26/dipeptidyl peptidase 4 (hDPP4), a functional receptor  
30 for MERS-CoV, under the control of an endogenous hDPP4 promoter. We then  
31 characterized this mouse model of MERS-CoV. The expression profile of hDPP4 in these  
32 mice was almost equivalent to that in human tissues, including kidney and lung; however,  
33 hDPP4 was overexpressed in murine CD3-positive cells within peripheral blood and  
34 lymphoid tissues. Intranasal inoculation of young and adult Tg mice with MERS-CoV led  
35 to infection of the lower respiratory tract and pathological evidence of acute multifocal  
36 interstitial pneumonia within 7 days, with only transient loss of body weight. However, the  
37 immunopathology in young and adult Tg mice was different. On Day 5 or 7  
38 post-inoculation, lungs of adult Tg mice contained higher levels of pro-inflammatory  
39 cytokines and chemokines associated with migration of macrophages. These results suggest  
40 that the immunopathology of MERS infection in the Tg mouse is age-dependent. The  
41 mouse model described herein will increase our understanding of disease pathogenesis and  
42 host mediators that protect against MERS-CoV infection.

43

44 **IMPORTANCE**

45 Middle East respiratory syndrome coronavirus (MERS-CoV) infections are endemic  
46 in the Middle East and a threat to public health worldwide. Rodents are not susceptible to  
47 the virus because they do not express functional receptors; therefore, we generated a new  
48 animal model of MERS-CoV infection based on transgenic mice expressing human  
49 (h)DPP4. The pattern of hDPP4 expression in this model was similar to that in human  
50 tissues (except lymphoid tissue). In addition, MERS-CoV was limited to the respiratory  
51 tract. Here, we focused on host factors involved in immunopathology in MERS-CoV  
52 infection and clarified differences in antiviral immune responses between young and adult  
53 transgenic mice. This new small animal model could contribute to more in-depth study of  
54 the pathology of MERS-CoV infection and aid development of suitable treatments.  
55

56 **INTRODUCTION**

57 Middle East respiratory syndrome coronavirus (MERS-CoV) was originally  
58 isolated as a novel coronavirus from a fatal case of acute respiratory distress syndrome  
59 and renal failure in 2012 (1). A human receptor for the virus, called human  
60 CD26/dipeptidyl peptidase 4 (hDPP4), was identified subsequently (2). Many  
61 epidemiological and virological investigations have been undertaken since then; however,  
62 information about the pathogenesis of MERS-CoV is limited. In addition, because  
63 MERS-CoV is endemic in the Middle East, the development of effective prophylactic  
64 and therapeutic treatment strategies remains a high priority. Therefore, appropriate  
65 animal models are needed to better understand the pathogenesis of MERS-CoV and  
66 facilitate development of effective vaccines and drugs. Some research groups  
67 experimentally infected nonhuman primates and small experimental animals with  
68 MERS-CoV (3-7). Rhesus macaques appear to develop a transient lower respiratory tract  
69 infection after a combination of intratracheal, ocular, oral, and intranasal inoculation with  
70 MERS-CoV (3), whereas the common marmoset develops progressive and severe  
71 pneumonia, which can be lethal (4). However, animal models based on nonhuman  
72 primates present both ethical and economic problems. Thus, establishing a small animal  
73 model of MERS-CoV infection is desirable. Unfortunately, MERS-CoV does not infect  
74 or replicate in small rodents such as Syrian hamsters (8), mice (9), or rats (10) because  
75 they lack a functional MERS-CoV receptor. Zhao *et al.* described lung infection in a

76 mouse model transduced with an adenovirus expressing hDPP4 (11); thus a transgenic  
77 (Tg) mouse carrying hDPP4 should be suitable for MERS-CoV studies (5). Some  
78 research groups developed Tg mice overexpressing the hDPP4 receptor under the control  
79 of CAG or cytokeratin 18 promoters (5-7). These mice developed severe lung disease,  
80 along with infection of the brain. Autopsy data are available from only one MERS  
81 patient; therefore, it is unclear whether MERS-CoV causes a systemic infection, although  
82 there is no evidence that MERS-CoV infects the human brain. Other studies describe  
83 development of a hDPP4 knock-in mouse (12-14). Although the tissue distribution and  
84 expression levels of hDPP4 in these models are largely equivalent to those of DPP4 in  
85 wild-type mice, the phenotype that determines MERS-CoV susceptibility varies from  
86 model to model. The hDPP4 knock-in mouse model described by Coleman *et al.* (12)  
87 succumbed to infection with wild-type MERS-CoV. By contrast, model mice described  
88 by Cockrell *et al.* (14) and Li *et al.* (13) are susceptible to infection by serially passaged  
89 MERS-CoV, which induces severe lung pathology and diffuse alveolar damage (DAD).  
90 These mice would be good models for studying pathogenesis of MERS. Here, we  
91 developed a new Tg mouse model expressing hDPP4 under the control of its endogenous  
92 promoter to better mimic physiological expression of hDPP4. These Tg mice were then  
93 backcrossed onto Th1-prone C57BL/6 mice. After evaluating susceptibility to  
94 MERS-CoV infection, we investigated age-dependent differences in disease  
95 pathogenesis; because older age is one of the common factors related to MERS severity,

96 and mortality (15-20). Both young and adult Tg mice infected with MERS-CoV showed  
97 transient weight loss along with moderate pneumonia and MERS-CoV replication in the  
98 lung; however, they did not recapitulate the severe disease and lethal infection seen in  
99 humans. Young and adult Tg mice infected with MERS-CoV did, however, show  
100 differing immunopathology. Adult Tg mice showed higher levels of pro-inflammatory  
101 cytokine- and chemokine-mediated macrophage infiltration of the lungs than young Tg  
102 mice. Taken together, these results suggest that age affects the immunopathology of  
103 MERS-CoV infection in Tg mice. The data suggest that other factors are required to  
104 recapitulate severe human disease in these Tg mice; however, this mouse model will be  
105 useful for identifying host mediators that protect against MERS-CoV infection. This  
106 animal model will provide new insight into factors that cause severe MERS-CoV  
107 infection.

108

## 109 **RESULTS**

### 110 **Expression of hDPP4 in Tg mouse tissues**

111 To generate Tg mice showing tissue- or cell type-specific hDPP4 expression  
112 mimicking that in humans, we first looked at research involving Tg mice harboring human  
113 enterovirus receptors (such as the human poliovirus receptor) and SCARB2 receptor-driven  
114 endogenous promoters (21, 22). Promoter sequences, which normally include a  
115 transcriptional start site, are usually isolated from the upstream regions of endogenous

116 mammalian genes (23). Therefore, we used a bacterial artificial chromosome (BAC) clone  
117 (RP11-345J9) containing the complete hDPP4 gene and an endogenous promotor to  
118 generate Tg mice harboring hDPP4 (Fig. 1A). To screen the generated Tg mice, we  
119 confirmed presence of the transgene by PCR genotyping using two primers sets specific for  
120 hDPP4 (Table 1; exon 3 and exon 10). hDPP4 is a protease expressed on the surface of cells  
121 in various organs, including T cells (24, 25). The enzyme is expressed by approximately  
122 60% of resting T cells isolated from blood (26). Since handling of peripheral blood in a  
123 laboratory is relatively simple, we conducted flow cytometry analysis using a  
124 FITC-conjugated anti-human CD26/hDPP4 monoclonal antibody that does not react with  
125 murine DPP4 to detect expression of hDPP4 in mice. CD3-positive lymphocytes from 2/15  
126 tested pups were positive for hDPP4. These mice were then crossed with C57BL/6 mice to  
127 establish two independent Tg lines (Tg1 and Tg2), which were maintained as hemizygotes  
128 carrying the hDPP4 gene. The Tg animals were born at the expected Mendel's ratio and  
129 were outwardly indistinguishable from control littermates. Because CD3-positive  
130 lymphocytes from peripheral blood of line Tg2 showed higher hDPP4 expression than those  
131 from line Tg1 (Fig. 1B), Tg2 was used for further analyses. PCR genotyping using primer  
132 sets specific for hDPP4 revealed that the complete hDPP4 gene had integrated into the  
133 genome of Tg2 mice (Fig. 1C, Table 1).

134 To examine hDPP4 expression in human and Tg2 tissues, we first performed  
135 Western blot analysis with a goat anti-CD26/hDPP4 polyclonal antibody (AF1180; R&D

136 Systems), which detected hDPP4 but cross-reacted weakly with mouse DPP4. Bands of  
137 about 110 kDa (hDPP4) were detected in all tested human tissues (liver, spleen, kidney,  
138 heart, lung, stomach, small intestine, large intestine, pancreas, brain, spinal cord, and  
139 skeletal muscle), except brain (Fig. 2A). All of the tissues from hDPP4 Tg mice expressed  
140 hDPP4, including liver, spleen, kidney, heart, lung, stomach, small intestine, large intestine,  
141 pancreas, brain, spinal cord, and skeletal muscle (Fig. 2A). These results suggest that the  
142 human transgene was expressed in the majority of organs/tissues in Tg2 mice.

143 To further determine hDPP4 distribution in tissues, immunohistochemistry (IHC)  
144 was performed (Fig. 2B). IHC using a goat anti-CD26/hDPP4 antibody detected hDPP4  
145 antigens in pneumocytes in the lung, in bile capillaries in the liver, in renal tubular  
146 epithelium, on the surface of epithelial cells lining the small intestine, in pancreatic islets,  
147 in lymphocytes in the lymph nodes, and in several types of endothelial cell and serous  
148 membranes (Fig. 2B, left column). While hDPP4 expression was undetectable in brain  
149 tissue by Western blot analysis, IHC revealed that endothelial cells lining blood vessels and  
150 leptomeninges of the human brain were positive for hDPP4, although neurons and glia were  
151 negative. In Tg2 mice, pneumocytes and bronchial epithelial cells in the lungs, bile  
152 capillaries in the liver, the renal tubular epithelium, and the surface of epithelial cells in the  
153 small intestine were positive for hDPP4 (Fig. 2B, middle column). In addition, several  
154 types of endothelial cells and serous membranes in all tested tissues, including the central  
155 nervous system, from Tg2 mice were positive for hDPP4. Notably, most lymphocytes in

156 the T cell zones of the spleen and lymph nodes from Tg2 mice were positive for hDPP4.  
157 Staining of tissues from non-Tg mice was very weak or absent (except for the small  
158 intestine) (Fig. 2B, right column). These data suggest that the pattern of hDPP4 expression  
159 in Tg2 mice is similar to that in humans (except for pancreas and lymphoid tissues).

160 Expression of hDPP4 was higher in lymphocytes from Tg2 mice than in those from  
161 humans (Fig. 1C and Fig. 2B). Therefore, we investigated the immune response profile in  
162 Tg2 mice. To assess innate immune responses in the lungs of Tg2, non-Tg, and C57BL/6  
163 mice, all animals received intranasal administration of PBS with or without poly(I:C), a  
164 synthetic analog of double-strand RNA (Fig. 3). There was no statistically significant  
165 difference in cytokine expression between Tg2, non-Tg, and C57BL/6 mice at 24 h after  
166 inoculation with poly(I:C) or PBS (Fig. 3). However, when we set expression levels after  
167 PBS treatment as 1, we noted that expression of MIP-1 $\alpha$ , GM-CSF, IL-1 $\beta$ , IL-12, and IL-2  
168 in poly(I:C)-treated Tg2 mice was 0.8–2-fold higher than in the other two strains. These  
169 results suggest that hDPP4 expression in mice does not have a marked effect on basal  
170 innate immune responses in the three mouse strains; however, Tg2 show slightly stronger  
171 or earlier innate immune responses than C57BL/6 mice and non-Tg mice. Thus, when we  
172 investigated immune responses in this animal model we made comparisons between  
173 MERS-CoV-infected and non-infected Tg mice.

174

#### 175 **Susceptibility of hDPP4-Tg mice to MERS-CoV infection**

176 In this experiment, C57BL/6 mice were used instead of non-Tg mice, because we  
177 were unable to prepare a sufficient number of non-Tg mice from littermate mice for this  
178 experiment. After intranasal inoculation of 10-week-old Tg2 and C57BL/6 mice with  $10^5$   
179 TCID<sub>50</sub> (50% of the tissue culture infectious dose) of MERS-CoV, neither group was  
180 lethargic; however, Tg2 mice showed mild but transient weight loss from Days 6 to 7  
181 post-inoculation (p.i.) (Tg2 mice, n = 8 [four females and four males]; and C57BL/6 mice,  
182 n = 10 [five female and five male]; Fig. 4A). Tg2 mice showed seroconversion at 35 days  
183 p.i., whereas C57BL/6 mice did not (Tg2 mice, n = 5 [three females and two males]; and  
184 C57BL/6 mice, n = 6 [three females and three males]; Fig. 4B), suggesting that Tg2 mice  
185 are susceptible to infection by MERS-CoV.

186 We next examined viral replication kinetics and sites of viral replication in  
187 10-week-old Tg2 and C57BL/6 mice (n = 3–4 [two females and 1–2 males per time point]).  
188 Tg2 mice and C57BL/6 mice were inoculated intranasally with  $10^5$  TCID<sub>50</sub> of MERS-CoV,  
189 and tissue specimens (the maxilla [including the nostril], nasal wash fluid, lung, and lung  
190 wash fluid) were collected at 6 h p.i. and on Days 1, 3, 5, and 7 p.i. The nasal wash fluid  
191 from three out of four Tg2 mice contained barely detectable levels of infectious virus at  
192 Days 1 and 5 p.i. (Fig. 4C). Supernatants from maxilla tissue homogenates (20%) from Tg2  
193 mice contained  $10^{2.8}$  TCID<sub>50</sub>/g at Day 1 p.i., although the titer fell by 5 days p.i. The viral  
194 titers in lung wash fluid and supernatants of lung tissue homogenates (20%) from Tg2 mice  
195 contained  $10^{2.3}$  TCID<sub>50</sub>/ml and  $10^{4.6}$  TCID<sub>50</sub>/g, respectively, at 1 day p.i.; these values were

196 significantly higher than those at 6 h p.i. ( $P < 0.05$  and  $P < 0.01$ , respectively; one-way  
197 ANOVA). The virus titers in the lungs were detectable up until 5 days p.i. Virus was  
198 undetectable in the respiratory tract at 7 days p.i. Although IHC revealed that various  
199 organs from Tg2 mice were positive for the hDPP4 antigen (Fig. 2B), no infectious virus  
200 was detected in the liver, spleen, kidney, heart, intestines, and brain up to 7 days p.i. (Table  
201 2). By contrast, virus was detected in the respiratory tract of C57BL/6 mice at 6 h p.i. only.  
202 These observations suggest that MERS-CoV infects and replicates mainly in the lower  
203 respiratory tract of Tg2 mice and is eliminated within 7 days of infection.

204         Several research groups have developed Tg mouse models of MERS-CoV infection;  
205 however, in these models, viral replication and MERS-CoV RNA were detected in the  
206 brain (5-7, 27). Thus, we next measured the amount of viral RNA in the brain of Tg2 mice  
207 at 6 h and at 1, 3, 5, and 7 days p.i. by real-time RT-PCR using primers specific for  
208 MERS-CoV; however, no MERS-CoV RNA was detected in the brain of Tg2 mice.  
209 Furthermore, another study showed that experimental infection of common marmosets with  
210 MERS-CoV resulted in viremia (4). Quantitative examination of viral RNA levels in Tg2  
211 mice revealed very low copy numbers of viral RNA in the blood at 3 and 5 days p.i., while  
212 sera from Tg2 mice were negative for the virus (Table 2). These results suggest that,  
213 although intranasal inoculation of Tg2 mice with MERS-CoV causes no neuroinvasion, it  
214 may induce viremia.

215 Several animal studies have identified MERS-CoV RNA in the lymphoid organs of  
216 infected animals (3, 4, 28), but no infectious virus was detected in the spleen from Tg2  
217 mice up to 7 days p.i. (Table 2). To investigate whether lymphoid organs in Tg2 mice are  
218 susceptible to MERS-CoV infection, we harvested splenocytes from Tg2 and C57BL/6  
219 mice and estimated infectivity and MERS-CoV RNA levels (Fig. 4D). Although the  
220 amount of infectious MERS-CoV in splenocytes was below the detection limit, viral RNA  
221 was detected in splenocytes from Tg2 mice (peaking at 2 days p.i.). Thus, lymphoid organs  
222 of Tg2 mice were as susceptible to MERS-CoV infection as those reported in other animal  
223 studies, although lymphoid organs were not a major site of MERS-CoV replication in Tg2  
224 mice after intranasal inoculation.

225

#### 226 **Acute inflammatory changes in the lungs of hDPP4-Tg mice after MERS-CoV** 227 **inoculation**

228 MERS-CoV infection of the nasal cavity, lungs, brain, spinal cord, liver, spleen,  
229 kidney, heart, and gastrointestinal tract of Tg2 mice was examined histopathologically on  
230 Days 1, 3, 5, 7, 14, and 35 p.i (n = 3 [one or two females and one or two males per time  
231 point]). Histopathological investigations revealed that Tg2 mice showed progressive  
232 pulmonary inflammation associated with acute virus infection, from which they recovered  
233 (Fig. 5). On Day 1 p.i., there was no obvious infiltration of the lungs in Tg2 mice; however,  
234 mild cellular degeneration and viral antigen-positive cells were seen in the bronchioles and

235 a few alveolar areas (Fig. 5A–C). Double immunofluorescence staining revealed that  
236 MERS-CoV antigen co-localized with hDPP4-positive bronchioles and alveolar cells on  
237 Day 1 p.i. (Fig. 6). On Days 3 and 5 p.i., inflammatory reactions, including partial and/or  
238 mild perivascular and peribronchiolar infiltration by mononuclear cells and eosinophils in  
239 response to viral antigens, were observed in alveolar areas of lung tissue from Tg2 mice  
240 (Fig. 5D–I). From Day 3 p.i. onwards, the alveolar area was the main site of inflammatory  
241 responses to viral replication (Fig. 5F, I, L). On Day 7 p.i., the point at which Tg2 mice  
242 showed weight loss, there was evidence of severe lung inflammation, including  
243 perivascular and alveolar septal thickening, caused by infiltrating mononuclear cells; some  
244 alveoli were positive for viral antigens (Fig. 5K). At Day 14 p.i., focal cellular infiltration  
245 was still evident in the peribronchioles and alveolar septa, although viral antigens and  
246 inflammatory responses had cleared from the lungs by Day 35 p.i. (Fig. 5M–P). There was  
247 no evidence of diffuse alveolar damage in the lungs up to Day 35 p.i. These findings  
248 suggest that progressive immunopathology occurred uniformly throughout the lungs, but  
249 resolved within 14 days after infection. Neither histopathology nor IHC detected  
250 inflammatory infiltration or viral antigens in the nasal cavity through 35 days p.i. In  
251 addition, there was no inflammation or viral antigen expression in the brain through 35  
252 days p.i. (Fig. 7). By contrast, C57BL/6 mice showed no histopathological changes or viral  
253 antigen in any organ, including the lung. These results indicate that Tg2 mice suffer acute  
254 pneumonia after infection of the lungs with MERS-CoV, which is related to expression of

255 hDPP4 in the bronchiolar epithelium and pneumocytes. Splenocytes from Tg2 mice were  
256 susceptible to *ex vivo* infection with MERS-CoV (Fig. 4D); however, the spleen and other  
257 lymphoid tissues did not harbor viral antigens. Furthermore, MERS-CoV induced T cell  
258 apoptosis upon infection *in vitro* (28), whereas immunohistochemical staining detected no  
259 evidence of apoptosis in lymphoid tissues, including spleen and lymph nodes, of  
260 MERS-CoV-infected Tg2 mice. Similar to the other mouse models in which mouse DPP4  
261 was replaced with hDPP4 (12), MERS-CoV replication and pathology were localized in the  
262 lungs of Tg2 mice.

263

264 **Differences in the immunopathology of MERS-CoV infection between young and**  
265 **adult hDPP4-Tg mice**

266 According to an epidemiological study (29), age (> 45 years) is considered to be one  
267 of the risk factors for MERS-CoV infection in humans. Therefore, we infected 25-week-old  
268 mice with MERS-CoV. Tg2 mice showed significant weight loss from Days 7 and 8 p.i.,  
269 before recovering by Day 14 p.i. (n = 6 [one female and five male Tg2 mice] and n = 7  
270 [three female and four male non-Tg mice]; Fig. 8A). However, 25-week-old Tg2 mice  
271 showed no obvious clinical signs (such as respiratory illness and mortality). The  
272 25-week-old Tg2 mice had seroconverted by 35 days p.i., whereas the C57BL/6 mice had  
273 not (Fig. 8B). Next, we examined viral replication kinetics and sites of viral replication in  
274 25-week-old Tg2 and non-Tg mice (n = 4 [two females and two males per time point]). The

275 nasal wash fluid from one out of four Tg2 mice contained barely detectable levels of  
276 infectious virus at 1, 3, and 5 days p.i. (Fig. 8C). Supernatants from maxilla tissue  
277 homogenates (20%) from Tg2 mice contained  $10^{1.7}$  and  $10^{2.0}$  TCID<sub>50</sub>/g at 1 and 3 days p.i.,  
278 respectively, although the titer was undetectable at 5 days p.i. The viral titers in lung wash  
279 fluid from Tg2 mice were detectable up until 3 days p.i., while the supernatants from lung  
280 tissue homogenates (20%) from Tg2 mice showed a high viral load from 1 to 5 days p.i.;  
281 infectious virus was detectable up until 7 days p.i. Viral loads in the respiratory tract  
282 peaked at 3 days p.i.. Although no virus was detectable in the respiratory tract of  
283 10-week-old Tg mice at 7 days p.i., infectious virus was detected in the lungs of  
284 25-week-old Tg mice up until 5 days p.i. In addition, infectious virus was detected in the  
285 lungs of one of four 25-week-old Tg mice ( $10^{2.5}$  TCID<sub>50</sub>/g) even at 7 days p.i. We also  
286 found that viral titers in the nasal wash fluid, maxilla (including nostril), lung wash fluid,  
287 and lungs of 25-week-old Tg2 mice on Day 3 p.i. ( $10^{2.6}$ /ml,  $10^{3.3}$ /ml,  $10^{2.3}$ /ml, and  $10^{4.9}$ /ml,  
288 respectively) were slightly higher than those in 10-week-old Tg2 mice ( $10^{1.6}$ /ml,  $10^{2.9}$ /ml,  
289  $10^{1.8}$ /ml, and  $10^{4.5}$ /ml, respectively) ( $P = 0.04$ , Student's *t* test with Welch's correction).

290 Histopathological analysis revealed that 25-week-old Tg2 mice showed delayed and  
291 prolonged inflammatory responses in the lung compared with those in 10-week-old Tg2  
292 mice (Fig. 9). Interestingly, viral antigen-positive cells were seen in the alveolar area on  
293 Day 1 p.i., and then in the bronchi on Day 3 p.i., along with a sparse cellular infiltrate (Fig.  
294 9A–F). Cellular infiltration (which included mononuclear cells and polynuclear cells) was

295 observed in the alveoli from 5 days p.i.; this expanded on Day 7 p.i. (Fig. 9G–L). Focal cell  
296 infiltration was seen in the alveoli on Day 14 p.i., and lymphoid cell aggregates were seen  
297 around bronchioles and blood vessels on Day 35 p.i. (Fig. 9M–R).

298 Next, we compared inflammation of the alveoli in 10-week-old Tg mice and  
299 25-week-old Tg mice on Day 7 p.i. Ionized calcium binding adaptor molecule 1 (Iba-1) is  
300 expressed specifically by monocytes/macrophages and is upregulated when these cells are  
301 activated. The predominant inflammatory infiltrate within the lungs of both 10-week-old  
302 and 25-week-old Tg mice comprised Iba-1-positive large cells and CD3-positive  
303 mononuclear cells (Fig. 10). Phagocytic vacuoles were prominent in large Iba-1 positive  
304 cells from 25-week-old Tg mice.

305

### 306 **Expression of pro-inflammatory cytokines and chemokines in hDPP4-Tg mice after**

### 307 **MERS-CoV infection**

308 Dysregulated cytokine and chemokine expression is observed in  
309 MERS-CoV-infected patients (30). Therefore, we measured the levels of 20 cytokines and  
310 chemokines in lung samples from both 10-week-old and 25-week-old Tg2 mice inoculated  
311 with either MERS-CoV or minimal essential medium (MEM). Measurements were made at  
312 6 h, and at 1, 3, 5, and 7 days, p.i. (n = 3–4 [two females and 1–2 males per time point], Fig.  
313 11A; and n = 4 [two females and two males per time point], Fig. 11B). On Day 3 p.i., we  
314 observed early expression of gamma IFN-induced protein 10 (IP-10) in the lungs of both

315 10- and 25-week-old Tg2 mice, which was significantly higher than that in control mice;  
316 this increase lasted through Day 7. This was followed by a transient increase in expression  
317 of interleukin (IL)-6, IL-13, and monocyte chemotactic protein-1 (MCP-1) in lungs from  
318 both 10- and 25-week-old Tg2 mice at Day 5 p.i. High levels of macrophage inflammatory  
319 protein 1 alpha (MIP-1 $\alpha$ ) and monokine induced by gamma IFN (MIG) were detected in  
320 the lungs of both groups of Tg2 mice from Days 3 or 5 to 7 p.i., whereas IL-12 levels  
321 increased at Day 7 p.i. IFN- $\gamma$  production in the lungs of 10-week-old Tg2 mice peaked  
322 significantly on Day 5 p.i. while high values were seen in both infected and non-infected  
323 25-week-old mice during the observation period. By contrast, expression of IP-10, IL-12,  
324 and IL-1 $\beta$  in 25-week-old Tg mice was higher than that in 10-week-old Tg2 mice.  
325 Interestingly, IL-1 $\alpha$  and IL-17 were detected only in 25-week-old Tg2 mice infected with  
326 MERS-CoV. IL-1 $\alpha$ , a potent pro-inflammatory cytokine associated with inflammation and  
327 fever, was detected from 3 days p.i. and remained significantly elevated until 7 days p.i.;  
328 IL-17 (a pro-inflammatory cytokine that recruits monocytes and neutrophils) was detected  
329 from 3 days p.i., peaking at 5 days p.i. before falling at 7 days p.i. These results indicate  
330 that MERS-CoV infection induces production of acute inflammatory chemokines and  
331 cytokines in the lungs. In addition, aging causes more severe immunopathology; this means  
332 that young and adult Tg mice show differing pathology in the lung after MERS-CoV  
333 infection.

334 Furthermore, we measured expression of mRNA encoding interferon (IFN)- $\alpha$ 4 and

335 IFN- $\beta$  (type 1 IFN with antiviral activity) in the lungs of 10- and 25-week-old mice at 6 h  
336 and at 1, 3, 5, and 7 days p.i. by real-time reverse transcription RT-PCR (31). We did not  
337 find any evidence of IFN- $\alpha$ 4 or IFN- $\beta$  in the lungs from 10-week-old Tg2 mice at early  
338 times post-infection; however, we observed a transient increase in IFN- $\alpha$ 4 expression in the  
339 lungs of two out of four Tg2 mice at 5 days p.i.; this fell by 7 days p.i. (Fig. 11C). Day 5 p.i.  
340 was the time point at which the amount of virus in the lungs of Tg2 mice began to fall. No  
341 IFN- $\beta$  mRNA was detectable in lung samples from either group. On the other hand, the  
342 lungs of 25-week-old Tg2 mice showed a transient increase in IFN- $\alpha$ 4 and IFN- $\beta$  mRNA  
343 expression at 3 days p.i. (Fig. 11C). In addition, IFN- $\alpha$ 4 and IFN- $\beta$  mRNA expression was  
344 higher than that in 10-week-old Tg2 mice. Taken together, these results indicate that both  
345 type 1 and type 2 IFN contribute to the immunopathology of the lungs of 25-week-old Tg2  
346 mice infected with MERS-CoV.

347

## 348 **DISCUSSION**

349 Here, we describe a new hDPP4-Tg mouse expressing the human gene under the  
350 control of an endogenous human promoter. This mouse model shows a pattern of hDPP4  
351 expression that closely mimics that in human tissues and is similar to that in other recent  
352 models (5-7). This mouse model also shows susceptibility to infection by MERS-CoV; this  
353 mimics the non-lethal observations in other mouse models (13, 14). After intranasal  
354 inoculation with a human isolate of MERS-CoV, the Tg mice developed acute and mild

355 interstitial pneumonia; however, the infection was non-lethal and so did not mimic severe  
356 cases seen in human MERS-CoV patients. MERS-CoV infection can cause severe illness,  
357 resulting in acute respiratory distress syndrome, although a large number of MERS-CoV  
358 infections follow a mild or asymptomatic course in healthy individuals (32-35). Thus, this  
359 Tg mouse model reflects the natural course of a mild MERS-CoV infection.

360         The majority of severe MERS-CoV cases occur in middle-aged and older males (36,  
361 37). Therefore, we infected Tg2 mice aged 25 weeks with MERS-CoV. The mice showed  
362 prominent pro-inflammatory responses and prolonged pulmonary inflammation when  
363 compared with Tg2 mice aged 10 weeks. However, none of the infected Tg2 mice had a  
364 severe outcome, such as respiratory distress, that led to death. Epidemiologically, patients  
365 with diabetes, kidney failure, or chronic lung disease, all of which might weaken the  
366 immune system, tend to have a poor outcome after infection by MERS-CoV  
367 (<http://www.who.int/csr/don/23-september-2015-mers-kuwait/en/>). Thus, it is presumed  
368 that a combination of older age and underlying disease might also increase mortality in this  
369 animal model.

370         This hDPP4-Tg mouse model, which lacks the clinical signs and mortality  
371 associated with severe MERS-CoV infection, is likely to be less advantageous than other  
372 lethal mouse models with respect to development of novel vaccines or antiviral agents  
373 (12-14). When we asked why the Tg2 mice showed non-lethal responses to infection, we  
374 could not ignore the fact that virus levels in lungs were lower than those reported for other

375 MERS mouse models (5, 12, 13, 38, 39). One reason for this is that the transgene used in  
376 this study is a hemizygote, meaning that the copy number or expression level may be lower  
377 than that in mice homozygous for hDPP4. In addition, the DPP4 protein is active as a dimer  
378 (40), but the Tg2 mice harbor both murine and hDPP4. We presume that the viral yield in  
379 the lungs of Tg2 mice was low because of heterodimers formed by hDPP4 and murine  
380 DPP4. To address this, we constructed structural models of homo- and heterodimers  
381 comprising human and mouse DPP4. Notably, the estimated interaction energy of the DPP4  
382 heterodimers was greater than that of murine and hDPP4 homodimers (-358.2, -347.6, and  
383 -344.6 kcal/mol, respectively). These results suggest that DPP4 heterodimers are as stable  
384 as DPP4 homodimers. Cockrell *et al.* reported that mouse DPP4 does not support  
385 MERS-CoV entry (38). Thus, the presence of stable DPP4 heterodimers may be a reason  
386 for the lower levels of infection in our mouse model. Further study is necessary to clarify  
387 this.

388           Some research groups generated a mouse-adapted MERS-CoV for use in  
389 severe/lethal MERS-CoV infection mouse models (13, 14). This may be one way to  
390 establish severe MERS infection in our Tg2 mice.

391           While the Tg2 mice expressed hDPP4 protein in the liver, spleen, kidney, heart,  
392 lung, gastrointestinal tract, pancreas, and brain, viral infection and replication were limited  
393 (mainly) to the lower respiratory tract, with little upper respiratory tract involvement, after  
394 intranasal inoculation of MERS-CoV. Tg2 mice developed interstitial pneumonia, and

395 MERS-CoV antigens were detected in the lungs. Virus yields in the lung were up to  
396 100-fold higher than those in the upper respiratory tract. Most MERS patients exhibit a  
397 severe lower respiratory tract infection, with little involvement of the upper respiratory tract  
398 (36). This suggests that MERS-CoV infection in Tg2 mice mimics mild infection in  
399 humans.

400 *In vitro* analysis of MERS-CoV suggests that the virus also infects human T cells  
401 and macrophages (28, 41, 42). We detected MERS-CoV RNA in serum and spleen cells  
402 from Tg2 mice. These data are similar to those generated from another Tg mouse model in  
403 which mouse DPP4 was replaced with hDPP4 under control of the endogenous mouse  
404 DPP4 promoter (12). MERS-CoV infection of T cells might affect immunopathology or  
405 induction of apoptosis in Tg mice, but we found no clear evidence of this. Although Tg2  
406 mice showed systemic viremia, infection of organs (except lung) did not lead to secondary  
407 complications. The disease phenotype (including clinical symptoms, viral titer in the lung,  
408 and acute pneumonia) appeared to be driven by infiltration by macrophages and  
409 lymphocytes; this is similar to the phenotype observed in another Tg mouse model  
410 harboring hDPP4 under the control of the endogenous mouse DPP4 promoter (12).

411 The Tg2 mice described herein did not show any brain or renal lesions after  
412 MERS-CoV infection. Other Tg mouse models in which hDPP4 is expressed under a strong  
413 ubiquitous promoter show high levels of viral RNA and inflammation in the lungs, which  
414 are accompanied by brain lesions (5, 7, 11). A fatal case of human MERS-CoV infection

415 published by Ng *et al.* showed no sign of MERS-CoV infection in the brain (43). To date,  
416 no reports suggest that MERS-CoV shows tropism for brain tissue. The primary target of  
417 MERS-CoV is the lower respiratory tract; however, patients with MERS often show signs  
418 of acute kidney failure (1, 43). In addition, MERS-CoV was identified in the urine of  
419 MERS patients (44, 45). Data from the first autopsy case did find pathological signs in the  
420 patient's kidneys, although IHC revealed no evidence of MERS-CoV replication in the  
421 kidneys (43). In addition, acute renal failure in this patient was not caused by MERS-CoV  
422 directly; rather, it was caused by hypotension (43) and/or acute respiratory distress  
423 syndrome (46).

424         Histopathological analysis identified CD3-positive T cells and Iba-1-positive  
425 macrophages in the lungs of Tg2 mice on Day 7 p.i., which correlated with expression of  
426 inflammatory cytokines and inflammatory infiltrates in the lung. Tg2 mice aged 10 and 25  
427 weeks showed increased expression of cytokines and chemokines associated with migration  
428 of T cells and activation of macrophages, including IP-10, IL-6, IL-13, MCP-1, IFN- $\gamma$ ,  
429 MIP-1 $\alpha$ , MIG, and IL-12, in the lungs at Days 5 and/or 7 p.i. This result is the same as that  
430 observed in a hDPP4 knock-in mouse model reported by Coleman *et al.* (12). In this hDPP4  
431 knock-in mouse model, CD8<sup>+</sup> T cells and macrophages affected the course of  
432 MERS-CoV-induced disease (12). In addition, Tg2 mice expressed mRNA encoding the  
433 type 1 IFN, IFN- $\alpha$ 4, during the early phase of the MERS-CoV infection. Importantly, the  
434 pathogenic and immune response data from the knock-in mouse model and our own model

435 are similar. Thus, an acute inflammatory reaction (including production of type 1 and type  
436 2 IFNs) and infiltration by macrophages might clear the virus from the lung, thereby  
437 preventing progression to MERS. Interestingly, we detected IL-1 $\alpha$  and IL-17 in the lungs of  
438 25-week-old Tg2 mice, but not those of 10-week-old Tg2 mice, after MERS-CoV infection.  
439 Both IL-1 $\alpha$  and IL-17 are pro-inflammatory cytokines that attract monocytes and  
440 neutrophils; therefore, they may exacerbate immunopathology after infection. These  
441 findings support the notion that the severity of MERS-CoV infection is age-dependent. Age  
442 is one of the most common factors related to severity and mortality of MERS infection;  
443 however, the underlying pathology is unclear (47).

444 Many studies have examined immune responses of MERS patients (30, 48-52).  
445 Indeed, elevated serum levels of IL-6, IL-12, IP-10, and IFN- $\gamma$  are observed in patients  
446 during the early period after severe infection (48-51). In addition, a prominent  
447 pro-inflammatory Th1 and Th17 response, including production of IFN- $\gamma$ , TNF- $\alpha$ , IL-15,  
448 and IL-17, is seen in patients during the acute phase of MERS-CoV infection (52). By  
449 contrast, we found that administration of poly(I:C) to Tg2 mice induced a mild increase (or  
450 earlier induction) in innate immune responses when compared with those in C57BL/6 mice  
451 and non-Tg mice. This suggests that overexpression of hDPP4 might influence immune  
452 responses in Tg2 mice. Thus, we must exercise caution when assessing the relationship  
453 between immunopathology and outcome in patients and animal models of MERS-CoV;

454 however, pro-inflammatory responses seem to contribute to immunopathology during the  
455 acute phase of MERS-CoV infection, both in patients and mouse models.

456 In summary, we generated a hDPP4-Tg mouse model showing mild respiratory  
457 infection by MERS-CoV. While this Tg mouse has limitations as a model for human  
458 MERS (i.e., lower virus titer in the lungs and mild disease), the immunopathology seems to  
459 resemble a mild and early stage of infection in humans. Even though it has limitations, this  
460 Tg mouse model will increase our understanding of the mechanisms underlying  
461 MERS-CoV infection. Indeed, we recently used this mouse model to confirm a role for  
462 transmembrane protease serine type2 (TMPRSS2) during MERS-CoV infection (Naoko  
463 Iwata-Yoshikawa *et al.*, submitted). This animal model may provide new insight into  
464 disease pathogenesis and guide development of therapeutic interventions that mitigate  
465 MERS.

466

## 467 **MATERIALS AND METHODS**

468 **Ethics statements.** Experiments using recombinant DNA and pathogens were approved by  
469 the Committee for Experiments using Recombinant DNA and Pathogens at the National  
470 Institute of Infectious Diseases, Tokyo, Japan. All animal experiments were approved by  
471 the Animal Care and Use Committee of the National Institute of Infectious Diseases, and  
472 the NCGM Research Institute, and were conducted in accordance with institutional  
473 Guidelines for the Care and Use of Animals. All animals were housed in a Japan Health

474 Sciences Foundation-certified facility. All human samples used in this study were obtained  
475 from US Biomax, Inc., GeneTex, Inc., Alpha Diagnostics International, or Protein  
476 Biotechnologies. The protocols were approved by the Health Insurance Portability and  
477 Accountability Act (HIPAA) or Institutional Review Board (IRB).

478

479 **Cells and viruses.** MERS-CoV, HCoV-EMC 2012 strain, was kindly provided by Dr. Bart  
480 Haagmans and Dr. Ron Fochier (Erasmus Medical Center, Rotterdam, the Netherlands) and  
481 was used throughout the study. Vero E6 cells, purchased from the American Type Cell  
482 Collection (Manassas, VA), were cultured in Eagle's MEM containing 5% fetal bovine  
483 serum (FBS), 50 IU/ml penicillin G, and 50 µg/ml streptomycin (5% FBS-MEM). Stocks of  
484 MERS-CoV were propagated and titrated on Vero E6 cells and cryopreserved at -80°C.  
485 Viral infectivity titers are expressed as the TCID<sub>50</sub>/ml on Vero E6 cells and were calculated  
486 according to the Behrens-Kärber method. Work with infectious MERS-CoV was performed  
487 under biosafety level 3 conditions.

488

489 **Virus isolation and titration.** Lung wash fluids and liver, kidney, heart, spleen, intestine,  
490 and brain tissue samples from Tg2, non-Tg, and C57BL/6 mice were collected at the time  
491 of postmortem examination and stored at -80°C. Tissue homogenates (20% [w/v]) were  
492 prepared in 2% FBS-MEM, and samples were inoculated onto Vero E6 cell cultures, which  
493 were then examined for cytopathic effects (CPE) for 5 days. Blind-passage was performed

494 after freezing and thawing cells from the first- or second-round passages. If  
495 MERS-CoV-specific CPE were not observed in the first-, second- or third-round cultures,  
496 the samples were deemed negative for infectious virus. Viral infectivity titers were  
497 determined in Vero E6 cell cultures using the micro-titration assay described above.  
498  
499 **MERS-CoV neutralizing assay.** Blood was obtained from each mouse and allowed to clot.  
500 Sera were then obtained by centrifugation and inactivated by incubation at 56°C for 30 min.  
501 One hundred TCID<sub>50</sub> aliquots of MERS-CoV were incubated for 1 h in the presence or  
502 absence of mouse serum (serially diluted 2-fold) and then added to confluent Vero E6 cell  
503 cultures in 96-well microtiter plates. The presence of a viral CPE was determined on Day 5,  
504 and the titers of neutralizing antibody were determined as the reciprocal of the highest  
505 dilution at which no CPE was observed. The lowest and highest serum dilutions tested were  
506 1:2 and 1:512, respectively.  
507  
508 **Generation of hDPP4-Tg mice.** To generate Tg mice expressing hDPP4, a BAC vector  
509 carrying the hDPP4 gene (RP11-345J9) was purchased from Advanced GenoTechs Co.,  
510 Japan. The BAC DNA was purified using a Large-Construct Kit (Qiagen) according to the  
511 manufacturer's instructions and suspended in TE buffer (10 mM Tris·HCl and 0.1 mM  
512 EDTA, pH 7.5) at a concentration of 4 ng/μl. Tg mice were generated using standard  
513 procedures (23). The purified BAC clones were microinjected into the pronuclei of

514 fertilized eggs from BDF1×C57BL/6NCr mice (SLC Inc., Hamamatsu, Japan) and then  
515 transplanted into pseudopregnant ICR mice (SLC Inc.). Expression of the transgene was  
516 assessed by FACS analysis as described below. The Tg mice were then backcrossed onto  
517 C57BL/6NCr for five generations. After weaning, the mice were tested for Tg integration  
518 by PCR and FACS analysis. Briefly, genomic DNA isolated from ear punch tissues was  
519 subjected to PCR using hDPP4-specific primers (Table 2) and lymphocytes were isolated  
520 from blood taken from the tail vein. Lymphocytes were screened for hDPP4 protein  
521 expression by flow cytometry analysis. Tg mice and their non-Tg littermates were used for  
522 the MERS-CoV infection study.

523

524 **Flow cytometry analysis.** Blood was collected from the retro-orbital venous plexus under  
525 isoflurane anesthesia using heparinized capillary tubes. The samples were then treated with  
526 Red Blood cell lysis buffer (Sigma-Aldrich, St. Louis, MO) to remove erythroid cells. For  
527 immunofluorescence staining, cells were re-suspended in staining buffer (PBS containing  
528 2.5% FBS, 0.5 mM EDTA, 0.05% NaN<sub>3</sub>) and Fc-receptors were blocked by incubation for  
529 20 min on ice with an unlabeled anti-mouse CD16/CD32 monoclonal antibody (clone:  
530 2.4G2; Bay bioscience Co., Ltd., Kobe, Japan). After washing, the cells were stained for 30  
531 min with a FITC-labeled anti-hDPP4 antibody (clone: BA5b) or with a control antibody  
532 against mouse IgG2a (clone: MOPC-173; BioLegend, San Diego, CA) and an APC-labeled  
533 anti-human CD3 antibody (clone: 145-2C11; BioLegend). Cells were then washed and

534 analyzed on a FACSCalibur flow cytometer (BD Biosciences, San Jose, CA). Data were  
535 processed using Cell Quest software (BD Biosciences).

536

537 **Western blot analysis.** To examine expression of DPP4 in human tissues, human tissue  
538 lysates prepared from the liver, spleen, kidney, heart, lung, stomach, small intestine, large  
539 intestine, pancreas, and brain were purchased from Alpha Diagnostics International (San  
540 Antonio, TX). Human skeletal muscle lysates were purchased from Protein Biotechnologies  
541 (Ramona, CA) and used under IRB-approval protocols. To prepare protein samples from  
542 the Tg and non-Tg mouse organs, tissues were homogenized in 0.5 ml of RIPA buffer (50  
543 mM Tris/HCl [pH 7.5], 150 mM NaCl, 1% [v/v] Nonidet P40 [NP40], 0.5% Sodium  
544 deoxycholate, 0.1% SDS) containing a protease inhibitor mixture (Complete Mini; Roche  
545 Diagnostics, Basel, Switzerland) and the protein concentrations were measured using a  
546 Pierce™ BCA protein assay kit (Thermo Fisher Scientific Inc., Waltham, MA).  
547 Homogenates (equivalent to 5 µg of protein) were subjected to SDS/PAGE on 4–12%  
548 Bis-Tris Protein Gels (Thermo Fisher Scientific), followed by transfer to a PVDF  
549 membrane (Millipore Corp., Billerica, MA). After blocking, the membranes were incubated  
550 for 1 h with a goat anti-hDPP4 antibody (0.1 µg/ml, Cat# AF1180; R&D Systems, Inc.,  
551 Minneapolis, MN) or a rabbit anti-β-actin antibody (1 µg/ml, Cat# ab8227; Abcam,  
552 Cambridge, UK), followed by incubation with a donkey anti-goat HRP-conjugated  
553 antibody (Abcam) and an anti-rabbit HRP-conjugated antibody (Abcam). The bands were

554 detected by an Immobilon Western Chemiluminescent HRP Substrate (Millipore) and an  
555 LAS-3000 apparatus (FUJIFILM, Tokyo, Japan).

556

557 **Intranasal administration of poly(I:C).** Tg2, non-Tg, and C57BL/6 mice (10 weeks old)  
558 were anesthetized and received 20 µg of poly(I:C) (Invitrogen, San Diego, CA) in 20 µl of  
559 saline intranasally. The dose of poly(I:C) was determined from previous studies (53).

560 Control mice received saline alone. To evaluate production of cytokines and chemokines in  
561 the lung, mice were sacrificed at 1 day post-administration (n = 4 per group [two females  
562 and two males]) and lungs were collected. Inflammatory cytokine profiles in 20% (w/v)  
563 lung homogenates were detected using a commercial Mouse Cytokine 20-Plex antibody  
564 bead kit (Thermo Fisher Scientific), as described by the manufacturer.

565

566 **Inoculation of mice with MERS-CoV.** Tg2 and non-Tg mice (9–10 weeks or 25 weeks  
567 old), and Tg2-BALB mice (12–22 weeks old), were anesthetized and inoculated  
568 intranasally with  $1 \times 10^5$  TCID<sub>50</sub> (30 µl) of MERS-CoV. Body weight was measured daily  
569 for 14 days (n = 4–8 per group), and animals were sacrificed at 6 h and at 1, 3, 5, 7, 14, and  
570 35 days p.i. to analyze virus replication, hematological parameters, cytokine expression,  
571 and disease pathology (n = 3–6 per group). Clinical signs were observed up until 14 days  
572 p.i. All mock-infected mice were inoculated with 2% FBS-MEM and used as controls for  
573 all analyses involving mice aged 9–10 weeks.

574

575 **Histopathology and IHC.** Formalin-fixed paraffin-embedded normal human tissue  
576 sections were purchased from separate sources: liver, spleen, lung, trachea, small intestine,  
577 colon, pancreas, cerebrum, cerebellum, and skeletal muscle were obtained from US Biomax,  
578 Inc. (Rockville, MD), whereas kidney, heart, spinal cord, stomach, and lymph node were  
579 obtained from GeneTex, Inc. (Irvine, CA). These human tissues were collected under  
580 HIPAA-approved protocols. To obtain animal tissues, mice were anesthetized and perfused  
581 with 2 ml of 10% phosphate-buffered formalin and the lungs, liver, spleen, kidney, heart,  
582 gastrointestinal tract, salivary glands, and brain tissue were harvested and fixed. Fixed  
583 tissues were routinely embedded in paraffin, sectioned, and stained with hematoxylin and  
584 eosin. For IHC, antigen retrieval of formalin-fixed mouse tissue sections was performed by  
585 autoclaving at 121°C for 10 min in retrieval solution at pH 6.0 (Nichirei, Tokyo, Japan).  
586 hDPP4 and MERS-CoV antigens were detected using a standard immunoperoxidase  
587 method and a goat anti-hDPP4 antibody (R&D Systems), a rabbit anti-MERS-CoV  
588 nucleocapsid antibody (Cat# 40068-RP01; Sino Biological Inc., Beijing, China).  
589 For double staining of CD3 (T cells) and Iba-1 (macrophages) antigen, we used a rabbit  
590 anti-human CD3 antibody (Cat# 790-4341; Ventana Medical System Inc., Tucson, AZ) and  
591 a rabbit anti-human Iba-1 antibody (Cat# 019-19741; Wako Pure Chemical Industries, Ltd.,  
592 Osaka, Japan). DAB (Sigma-Aldrich Co., MO, USA) and the VINA Green Chromogen Kit  
593 (Biocare Medical, CA, USA) were used as chromogens for HRP visualization. Following

594 the first staining of CD3 using the polymer-based detection system with DAB, denaturing  
595 was performed by hydrolytic autoclaving in citrate buffer (pH 6.0) for 10 min at 121°C.  
596 The second staining was performed for Iba-1 with Vina Green. Nuclei were counterstained  
597 with hematoxylin for 10 sec. To detect apoptosis, TUNEL labeling was performed using the  
598 In Situ Cell Death Detection Kit (Roche).

599

600 **Quantitative real-time RT-PCR.** To measure the levels of type I IFN mRNA expression  
601 and the number of viral genome copies, RNA was extracted from 20% (w/v) lung and brain  
602 tissue homogenates and from the blood of Tg2 and non-Tg mice infected with MERS-CoV  
603 using RNeasy Mini kits (Qiagen, Hilden, Germany), according to the manufacturer's  
604 instructions. mRNA encoding IFN- $\alpha$ , IFN- $\beta$ , and the E gene of MERS-CoV was examined  
605 by real-time RT-PCR using an ABI Prism 7900HT Fast real-time PCR system (Applied  
606 Biosystems, Foster City, CA). The TaqMan probes and primers, and the reaction conditions,  
607 have been described previously (31). Expression of each gene was normalized to that of  
608  $\beta$ -actin.

609

610 **Detection of inflammatory cytokines and chemokines.** Cytokines and chemokines in  
611 mouse lung homogenates (10% w/v) were measured using a commercial Mouse Cytokine  
612 20-Plex antibody bead kit (Thermo Fisher Scientific). A panel of inflammatory cytokines  
613 and chemokines (basic fibroblast growth factor [bFGF], granulocyte-macrophage,

614 colony-stimulating factor [GM-CSF], IFN- $\gamma$ , IL-1 $\alpha$ , IL-1 $\beta$ , IL-2, IL-4, IL-5, IL-6, IL-10,  
615 IL-12p40/p70, IL-13, IL-17, IP-10, keratinocyte chemoattractant [KC], MCP-1, MIG,  
616 MIP-1 $\alpha$ , TNF- $\alpha$ , and vascular endothelial growth factor) was measured according to the  
617 manufacturer's protocols.

618

619 **Isolation of splenocytes and infection with MERS-CoV.** Spleens were removed

620 aseptically from Tg2 and C57BL/6 mice (n = 3 each), dissociated in RPMI-1640 medium,  
621 and pressed gently through a 40  $\mu$ m nylon mesh filter. The cell suspension was centrifuged  
622 at 400 g for 10 min, and red blood cells were lysed with blood cell lysis buffer (final  
623 concentration: 155 mM NH<sub>4</sub>Cl, 10 mM KHCO<sub>3</sub>, and 0.1 mM EDTA; pH 7.3) at room  
624 temperature for 5 min. The cells were washed twice with RPMI-1640 medium and  
625 centrifuged at 1000 g for 10 min. hDPP4-expressing CD3<sup>+</sup> T cells within the splenocyte  
626 population were detected by flow cytometry analysis. The percentage of CD3<sup>+</sup> T cells was  
627 39.11 $\pm$ 3.8%, and that of hDPP4-expressing CD3<sup>+</sup> T cells was 26.46 $\pm$ 1.9%. The cells were  
628 re-suspended in the medium and infected with MERS-CoV (MOI of 1). Viral replication  
629 was determined after 1 and 2 days of culture. Viral infectivity titers were measured in Vero  
630 E6 cell cultures using a micro-titration assay. To detect the MERS-CoV genome in  
631 splenocytes, RNA from splenocytes infected with MERS-CoV was extracted at 1 and 2  
632 days p.i. and subjected to quantitative real-time RT-PCR (10).

633

634 **Molecular modeling of DPP4 homo- and heterodimers.** DPP4 dimer models were  
635 constructed using the Molecular Operating Environment (MOE) (Chemical Computing  
636 Group Inc., Montreal, Quebec, Canada) based on the crystal structure of hDPP4 at a  
637 resolution of 2.55 Å (PDB code: 2ONC). Stereochemical quality was assessed using the  
638 Ramachandran Plot and Atom Clashes applications in MOE. Interaction energy, which is  
639 an indicator of the affinity of the dimer, was calculated using the Potential Energy  
640 application in MOE.

641

642 **Statistical analysis.** Data are expressed as the mean and standard error of the mean.

643 Statistical analyses were performed using Graph Pad Prism 5 software (GraphPad Software  
644 Inc., La Jolla, CA). Intergroup comparisons were performed using one-way, two-way  
645 ANOVA, or Student's *t* test with Welch's correction. A P-value < 0.05 was considered  
646 statistically significant.

647

#### 648 **FUNDING INFORMATION**

649 This work was supported by a Grant-in-Aid for research (H25-Shinko-Wakate-004)  
650 from the Ministry of Health, Labor, and Welfare, Japan, by a Research Program on  
651 Emerging and Re-emerging Infectious Diseases (JP17fk0108313, JP18fk0108058) from the  
652 Japan Agency for Medical Research and Development, AMED, by a Grant-in-Aid for  
653 scientific research from the Ministry of Education, Culture, Sports, Science, and

654 Technology in Japan, (KAKENHI; 16K09951, 18H02665), and in part by The Grant for  
655 National Center for Global Health and Medicine (27A1102).

656

657 **ACKNOWLEDGEMENTS**

658 We thank Drs. Bart Haagmans and Ron Fouchier for providing MERS-CoV (isolate  
659 HCoV-EMC/2012) and Drs. Satoshi Koike, Ken Fujii (Tokyo Metropolitan Institute of  
660 Medical Science), and Shutoku Matsuyama (National Institute of Infectious Diseases) for  
661 helpful discussion. We also thank Ms. Ayako Harashima and Midori Ozaki for technical  
662 assistance.

## 663 REFERENCES

- 664 1. **Zaki AM, van Boheemen S, Bestebroer TM, Osterhaus AD, Fouchier RA.**  
665 2012. Isolation of a novel coronavirus from a man with pneumonia in  
666 Saudi Arabia. *The New England journal of medicine* **367**:1814-1820.
- 667 2. **Raj VS, Mou H, Smits SL, Dekkers DH, Muller MA, Dijkman R, Muth D,**  
668 **Demmers JA, Zaki A, Fouchier RA, Thiel V, Drosten C, Rottier PJ,**  
669 **Osterhaus AD, Bosch BJ, Haagmans BL.** 2013. Dipeptidyl peptidase 4 is  
670 a functional receptor for the emerging human coronavirus-EMC. *Nature*  
671 **495**:251-254.
- 672 3. **de Wit E, Rasmussen AL, Falzarano D, Bushmaker T, Feldmann F,**  
673 **Brining DL, Fischer ER, Martellaro C, Okumura A, Chang J, Scott D,**  
674 **Benecke AG, Katze MG, Feldmann H, Munster VJ.** 2013. Middle East  
675 respiratory syndrome coronavirus (MERS-CoV) causes transient lower  
676 respiratory tract infection in rhesus macaques. *Proceedings of the*  
677 *National Academy of Sciences of the United States of America*  
678 **110**:16598-16603.
- 679 4. **Falzarano D, de Wit E, Feldmann F, Rasmussen AL, Okumura A, Peng X,**  
680 **Thomas MJ, van Doremalen N, Haddock E, Nagy L, LaCasse R, Liu T,**  
681 **Zhu J, McLellan JS, Scott DP, Katze MG, Feldmann H, Munster VJ.** 2014.  
682 Infection with MERS-CoV causes lethal pneumonia in the common  
683 marmoset. *PLoS pathogens* **10**:e1004250.
- 684 5. **Agrawal AS, Garron T, Tao X, Peng BH, Wakamiya M, Chan TS, Couch**  
685 **RB, Tseng CT.** 2015. Generation of a transgenic mouse model of Middle  
686 East respiratory syndrome coronavirus infection and disease. *Journal of*  
687 *virology* **89**:3659-3670.
- 688 6. **Zhao G, Jiang Y, Qiu H, Gao T, Zeng Y, Guo Y, Yu H, Li J, Kou Z, Du L,**  
689 **Tan W, Jiang S, Sun S, Zhou Y.** 2015. Multi-Organ Damage in Human  
690 Dipeptidyl Peptidase 4 Transgenic Mice Infected with Middle East  
691 Respiratory Syndrome-Coronavirus. *PloS one* **10**:e0145561.
- 692 7. **Li K, Wohlford-Lenane C, Perlman S, Zhao J, Jewell AK, Reznikov LR,**

- 693 **Gibson-Corley KN, Meyerholz DK, McCray PB, Jr.** 2016. Middle East  
694 Respiratory Syndrome Coronavirus Causes Multiple Organ Damage and  
695 Lethal Disease in Mice Transgenic for Human Dipeptidyl Peptidase 4.  
696 *The Journal of infectious diseases* **213**:712-722.
- 697 8. **de Wit E, Prescott J, Baseler L, Bushmaker T, Thomas T, Lackemeyer**  
698 **MG, Martellaro C, Milne-Price S, Haddock E, Haagmans BL, Feldmann**  
699 **H, Munster VJ.** 2013. The Middle East respiratory syndrome coronavirus  
700 (MERS-CoV) does not replicate in Syrian hamsters. *PloS one* **8**:e69127.
- 701 9. **Coleman CM, Matthews KL, Goicochea L, Frieman MB.** 2013. Wild type  
702 and innate immune deficient mice are not susceptible to the Middle East  
703 Respiratory Syndrome Coronavirus. *The Journal of general virology*.
- 704 10. **Iwata-Yoshikawa N, Fukushi S, Fukuma A, Suzuki T, Takeda M, Tashiro**  
705 **M, Hasegawa H, Nagata N.** 2016. No susceptibility of neonatal and adult  
706 rats against the Middle East respiratory syndrome coronavirus.  
707 *Japanese journal of infectious diseases*.
- 708 11. **Zhao J, Li K, Wohlford-Lenane C, Agnihothram SS, Fett C, Zhao J, Gale**  
709 **MJ, Jr., Baric RS, Enjuanes L, Gallagher T, McCray PB, Jr., Perlman S.**  
710 2014. Rapid generation of a mouse model for Middle East respiratory  
711 syndrome. *Proceedings of the National Academy of Sciences of the United*  
712 *States of America* **111**:4970-4975.
- 713 12. **Coleman CM, Sisk JM, Halasz G, Zhong J, Beck SE, Matthews KL,**  
714 **Venkataraman T, Rajagopalan S, Kyratsous CA, Frieman MB.** 2017.  
715 CD8+ T Cells and Macrophages Regulate Pathogenesis in a Mouse Model  
716 of Middle East Respiratory Syndrome. *Journal of virology* **91**.
- 717 13. **Li K, Wohlford-Lenane CL, Channappanavar R, Park JE, Earnest JT,**  
718 **Bair TB, Bates AM, Brogden KA, Flaherty HA, Gallagher T, Meyerholz**  
719 **DK, Perlman S, McCray PB, Jr.** 2017. Mouse-adapted MERS coronavirus  
720 causes lethal lung disease in human DPP4 knockin mice. *Proceedings of*  
721 *the National Academy of Sciences of the United States of America*  
722 **114**:E3119-E3128.

- 723 14. **Cockrell AS, Yount BL, Scobey T, Jensen K, Douglas M, Beall A, Tang XC,**  
724 **Marasco WA, Heise MT, Baric RS.** 2016. A mouse model for MERS  
725 coronavirus-induced acute respiratory distress syndrome. *Nature*  
726 *microbiology* **2**:16226.
- 727 15. **Korea Centers for Disease Control and Prevention.** 2015. Middle East  
728 Respiratory Syndrome Coronavirus Outbreak in the Republic of Korea,  
729 2015. *Osong public health and research perspectives* **6**:269-278.
- 730 16. **Saad M, Omrani AS, Baig K, Bahloul A, Elzein F, Matin MA, Selim MA,**  
731 **Al Mutairi M, Al Nakhli D, Al Aidaroos AY, Al Sherbeeni N, Al-Khashan**  
732 **HI, Memish ZA, Albarrak AM.** 2014. Clinical aspects and outcomes of 70  
733 patients with Middle East respiratory syndrome coronavirus infection: a  
734 single-center experience in Saudi Arabia. *International journal of*  
735 *infectious diseases : IJID : official publication of the International Society*  
736 *for Infectious Diseases* **29**:301-306.
- 737 17. **Ahmed AE.** 2017. The predictors of 3- and 30-day mortality in 660  
738 MERS-CoV patients. *BMC infectious diseases* **17**:615.
- 739 18. **Alsahafi AJ, Cheng AC.** 2016. The epidemiology of Middle East  
740 respiratory syndrome coronavirus in the Kingdom of Saudi Arabia,  
741 2012-2015. *International journal of infectious diseases : IJID : official*  
742 *publication of the International Society for Infectious Diseases* **45**:1-4.
- 743 19. **Majumder MS, Kluberg SA, Mekaru SR, Brownstein JS.** 2015. Mortality  
744 Risk Factors for Middle East Respiratory Syndrome Outbreak, South  
745 Korea, 2015. *Emerging infectious diseases* **21**:2088-2090.
- 746 20. **Choi WS, Kang CI, Kim Y, Choi JP, Joh JS, Shin HS, Kim G, Peck KR,**  
747 **Chung DR, Kim HO, Song SH, Kim YR, Sohn KM, Jung Y, Bang JH, Kim**  
748 **NJ, Lee KS, Jeong HW, Rhee JY, Kim ES, Woo H, Oh WS, Huh K, Lee YH,**  
749 **Song JY, Lee J, Lee CS, Kim BN, Choi YH, Jeong SJ, Lee JS, Yoon JH, Wi**  
750 **YM, Joung MK, Park SY, Lee SH, Jung SI, Kim SW, Lee JH, Lee H, Ki**  
751 **HK, Kim YS.** 2016. Clinical Presentation and Outcomes of Middle East  
752 Respiratory Syndrome in the Republic of Korea. *Infection &*

- 753 chemotherapy **48**:118-126.
- 754 21. **Koike S, Taya C, Kurata T, Abe S, Ise I, Yonekawa H, Nomoto A.** 1991.  
755 Transgenic mice susceptible to poliovirus. Proceedings of the National  
756 Academy of Sciences of the United States of America **88**:951-955.
- 757 22. **Fujii K, Nagata N, Sato Y, Ong KC, Wong KT, Yamayoshi S, Shimanuki**  
758 **M, Shitara H, Taya C, Koike S.** 2013. Transgenic mouse model for the  
759 study of enterovirus 71 neuropathogenesis. Proceedings of the National  
760 Academy of Sciences of the United States of America **110**:14753-14758.
- 761 23. **Haruyama N, Cho A, Kulkarni AB.** 2009. Overview: engineering  
762 transgenic constructs and mice. Current protocols in cell biology /  
763 editorial board, Juan S. Bonifacino ... [et al.] **Chapter 19**:Unit 19 10.
- 764 24. **Geppert TD, Davis LS, Gur H, Wacholtz MC, Lipsky PE.** 1990. Accessory  
765 cell signals involved in T-cell activation. Immunological reviews **117**:5-66.
- 766 25. **Fleischer B.** 1994. CD26: a surface protease involved in T-cell activation.  
767 Immunology today **15**:180-184.
- 768 26. **Hegen M, Niedobitek G, Klein CE, Stein H, Fleischer B.** 1990. The T cell  
769 triggering molecule Tp103 is associated with dipeptidyl aminopeptidase  
770 IV activity. J Immunol **144**:2908-2914.
- 771 27. **Fan C, Wu X, Liu Q, Li Q, Liu S, Lu J, Yang Y, Cao Y, Huang W, Liang C,**  
772 **Ying T, Jiang S, Wang Y.** 2018. A Human DPP4-Knockin Mouse's  
773 Susceptibility to Infection by Authentic and Pseudotyped MERS-CoV.  
774 Viruses **10**.
- 775 28. **Chu H, Zhou J, Wong BH, Li C, Chan JF, Cheng ZS, Yang D, Wang D, Lee**  
776 **AC, Li C, Yeung ML, Cai JP, Chan IH, Ho WK, To KK, Zheng BJ, Yao Y,**  
777 **Qin C, Yuen KY.** 2016. Middle East Respiratory Syndrome Coronavirus  
778 Efficiently Infects Human Primary T Lymphocytes and Activates the  
779 Extrinsic and Intrinsic Apoptosis Pathways. The Journal of infectious  
780 diseases **213**:904-914.
- 781 29. **Alghamdi IG, Hussain, II, Almalki SS, Alghamdi MS, Alghamdi MM,**  
782 **El-Sheemy MA.** 2014. The pattern of Middle East respiratory syndrome

- 783 coronavirus in Saudi Arabia: a descriptive epidemiological analysis of  
784 data from the Saudi Ministry of Health. *International journal of general*  
785 *medicine* **7**:417-423.
- 786 30. **van den Brand JM, Smits SL, Haagmans BL.** 2015. Pathogenesis of  
787 Middle East respiratory syndrome coronavirus. *The Journal of pathology*  
788 **235**:175-184.
- 789 31. **Iwata-Yoshikawa N, Uda A, Suzuki T, Tsunetsugu-Yokota Y, Sato Y,**  
790 **Morikawa S, Tashiro M, Sata T, Hasegawa H, Nagata N.** 2014. Effects of  
791 Toll-like receptor stimulation on eosinophilic infiltration in lungs of  
792 BALB/c mice immunized with UV-inactivated severe acute respiratory  
793 syndrome-related coronavirus vaccine. *Journal of virology* **88**:8597-8614.
- 794 32. **Memish ZA, Zumla AI, Assiri A.** 2013. Middle East respiratory syndrome  
795 coronavirus infections in health care workers. *The New England journal*  
796 *of medicine* **369**:884-886.
- 797 33. 2013. State of Knowledge and Data Gaps of Middle East Respiratory  
798 Syndrome Coronavirus (MERS-CoV) in Humans. *PLoS currents* **5**.
- 799 34. **O'Hagan JJ, Carias C, Rudd JM, Pham HT, Haber Y, Pesik N, Cetron MS,**  
800 **Gambhir M, Gerber SI, Swerdlow DL.** 2016. Estimation of Severe Middle  
801 East Respiratory Syndrome Cases in the Middle East, 2012-2016.  
802 *Emerging infectious diseases* **22**:1797-1799.
- 803 35. **Omrani AS, Matin MA, Haddad Q, Al-Nakhli D, Memish ZA, Albarrak**  
804 **AM.** 2013. A family cluster of Middle East Respiratory Syndrome  
805 Coronavirus infections related to a likely unrecognized asymptomatic or  
806 mild case. *International journal of infectious diseases : IJID : official*  
807 *publication of the International Society for Infectious Diseases*  
808 **17**:e668-672.
- 809 36. 2013. Update: Severe respiratory illness associated with Middle East  
810 Respiratory Syndrome Coronavirus (MERS-CoV)--worldwide, 2012-2013.  
811 *MMWR. Morbidity and mortality weekly report* **62**:480-483.
- 812 37. **Assiri A, Abedi GR, Bin Saeed AA, Abdalla MA, al-Masry M, Choudhry**

- 813 **AJ, Lu X, Erdman DD, Tatti K, Binder AM, Rudd J, Tokars J, Miao C,**  
814 **Alarbash H, Nooh R, Pallansch M, Gerber SI, Watson JT.** 2016.  
815 Multifacility Outbreak of Middle East Respiratory Syndrome in Taif,  
816 Saudi Arabia. *Emerging infectious diseases* **22**:32-40.
- 817 38. **Cockrell AS, Peck KM, Yount BL, Agnihothram SS, Scobey T, Curnes NR,**  
818 **Baric RS, Heise MT.** 2014. Mouse dipeptidyl peptidase 4 is not a  
819 functional receptor for Middle East respiratory syndrome coronavirus  
820 infection. *Journal of virology* **88**:5195-5199.
- 821 39. **Pascal KE, Coleman CM, Mujica AO, Kamat V, Badithe A, Fairhurst J,**  
822 **Hunt C, Strein J, Berrebi A, Sisk JM, Matthews KL, Babb R, Chen G, Lai**  
823 **KM, Huang TT, Olson W, Yancopoulos GD, Stahl N, Frieman MB,**  
824 **Kyratsous CA.** 2015. Pre- and postexposure efficacy of fully human  
825 antibodies against Spike protein in a novel humanized mouse model of  
826 MERS-CoV infection. *Proceedings of the National Academy of Sciences of*  
827 *the United States of America* **112**:8738-8743.
- 828 40. **Chien CH, Huang LH, Chou CY, Chen YS, Han YS, Chang GG, Liang PH,**  
829 **Chen X.** 2004. One site mutation disrupts dimer formation in human  
830 DPP-IV proteins. *The Journal of biological chemistry* **279**:52338-52345.
- 831 41. **Tynell J, Westenius V, Ronkko E, Munster VJ, Melen K, Osterlund P,**  
832 **Julkunen I.** 2016. Middle East respiratory syndrome coronavirus shows  
833 poor replication but significant induction of antiviral responses in human  
834 monocyte-derived macrophages and dendritic cells. *The Journal of*  
835 *general virology* **97**:344-355.
- 836 42. **Zhou J, Chu H, Li C, Wong BH, Cheng ZS, Poon VK, Sun T, Lau CC,**  
837 **Wong KK, Chan JY, Chan JF, To KK, Chan KH, Zheng BJ, Yuen KY.** 2014.  
838 Active replication of Middle East respiratory syndrome coronavirus and  
839 aberrant induction of inflammatory cytokines and chemokines in human  
840 macrophages: implications for pathogenesis. *The Journal of infectious*  
841 *diseases* **209**:1331-1342.
- 842 43. **Ng DL, Al Hosani F, Keating MK, Gerber SI, Jones TL, Metcalfe MG,**

- 843 **Tong S, Tao Y, Alami NN, Haynes LM, Mutei MA, Abdel-Wareth L, Uyeki**  
844 **TM, Swerdlow DL, Barakat M, Zaki SR.** 2016. Clinicopathologic,  
845 Immunohistochemical, and Ultrastructural Findings of a Fatal Case of  
846 Middle East Respiratory Syndrome Coronavirus Infection in the United  
847 Arab Emirates, April 2014. *The American journal of pathology*  
848 **186:652-658.**
- 849 44. **Poissy J, Goffard A, Parmentier-Decrucq E, Favory R, Kouv M, Kipnis E,**  
850 **Mathieu D, van der Werf S, Guery B.** 2014. Kinetics and pattern of viral  
851 excretion in biological specimens of two MERS-CoV cases. *Journal of*  
852 *clinical virology : the official publication of the Pan American Society for*  
853 *Clinical Virology* **61:275-278.**
- 854 45. **Drosten C, Seilmaier M, Corman VM, Hartmann W, Scheible G, Sack S,**  
855 **Guggemos W, Kallies R, Muth D, Junglen S, Muller MA, Haas W,**  
856 **Guberina H, Rohnisch T, Schmid-Wendtner M, Aldabbagh S, Dittmer U,**  
857 **Gold H, Graf P, Bonin F, Rambaut A, Wendtner CM.** 2013. Clinical  
858 features and virological analysis of a case of Middle East respiratory  
859 syndrome coronavirus infection. *The Lancet. Infectious diseases*  
860 **13:745-751.**
- 861 46. **Seeley EJ.** 2013. Updates in the management of acute lung injury: a focus  
862 on the overlap between AKI and ARDS. *Advances in chronic kidney*  
863 *disease* **20:14-20.**
- 864 47. **Park JE, Jung S, Kim A, Park JE.** 2018. MERS transmission and risk  
865 factors: a systematic review. *BMC public health* **18:574.**
- 866 48. **Faure E, Poissy J, Goffard A, Fournier C, Kipnis E, Titecat M, Bortolotti**  
867 **P, Martinez L, Dubucquoi S, Dessein R, Gosset P, Mathieu D, Guery B.**  
868 2014. Distinct immune response in two MERS-CoV-infected patients: can  
869 we go from bench to bedside? *PloS one* **9:e88716.**
- 870 49. **Guan WD, Mok CK, Chen ZL, Feng LQ, Li ZT, Huang JC, Ke CW, Deng X,**  
871 **Ling Y, Wu SG, Niu XF, Perera RA, Da Xu Y, Zhao J, Zhang LQ, Li YM,**  
872 **Chen RC, Peiris M, Chen L, Zhong NS.** 2015. Characteristics of Traveler

- 873 with Middle East Respiratory Syndrome, China, 2015. *Emerging*  
874 *infectious diseases* **21**:2278-2280.
- 875 50. **Min CK, Cheon S, Ha NY, Sohn KM, Kim Y, Aigerim A, Shin HM, Choi JY,**  
876 **Inn KS, Kim JH, Moon JY, Choi MS, Cho NH, Kim YS.** 2016.  
877 Comparative and kinetic analysis of viral shedding and immunological  
878 responses in MERS patients representing a broad spectrum of disease  
879 severity. *Scientific reports* **6**:25359.
- 880 51. **Shin HS, Kim Y, Kim G, Lee JY, Jeong I, Joh JS, Kim H, Chang E, Sim**  
881 **SY, Park JS, Lim DG.** 2018. Immune responses to MERS coronavirus  
882 during the acute and convalescent phases of human infection. *Clinical*  
883 *infectious diseases* : an official publication of the Infectious Diseases  
884 Society of America.
- 885 52. **Mahallawi WH, Khabour OF, Zhang Q, Makhdoum HM, Suliman BA.**  
886 2018. MERS-CoV infection in humans is associated with a  
887 pro-inflammatory Th1 and Th17 cytokine profile. *Cytokine* **104**:8-13.
- 888 53. **Ichinohe T, Watanabe I, Ito S, Fujii H, Moriyama M, Tamura S,**  
889 **Takahashi H, Sawa H, Chiba J, Kurata T, Sata T, Hasegawa H.** 2005.  
890 Synthetic double-stranded RNA poly(I:C) combined with mucosal vaccine  
891 protects against influenza virus infection. *Journal of virology*  
892 **79**:2910-2919.  
893

894 **FIGURE LEGENDS**895 **Fig. 1.** Generation of transgenic mice expressing human dipeptidyl peptidase 4 (hDPP4).

896 (A) Schematic diagram showing a bacterial artificial chromosome clone (BAC clone  
897 RP11-345G-9) containing the hDPP4 gene used to produce the transgenic mice. The open  
898 and closed circles denote the centromere (Cen) and telomere (Tel) of human chromosome 2,  
899 respectively. The gray arrows indicate the genes located downstream of the hDPP4 gene  
900 (white arrow). The cloned region in the BAC construct is denoted by a black line. GCG,  
901 glucagon gene; FAP, fibroblast activation protein; IFIH1, interferon induced with helicase  
902 C domain 1. (B) Expression of hDPP4 on peripheral blood CD3-positive T-lymphocytes  
903 from the transgenic (Tg) mice. Tg1 and Tg2, hDPP4<sup>+/+</sup> transgenic mouse lines 1 and 2;  
904 non-Tg, hDPP4<sup>-/-</sup> mouse. (C) Genomic DNA was extracted from Tg2 mice, and human  
905 DPP4 exons 1–26 were subjected to PCR using specific primers. M: marker; Lane 1: exon  
906 1; Lane 2: exon 2; Lane 3: exon 3; Lane 4: exon 4; Lane 5: exon 5; Lane 6: exon 6 to 7;  
907 Lane 7: exon 8; Lane 8: exon 9; Lane 9: exon 10; Lane 10: exon 11; Lane 11: exon 12;  
908 Lane 12: exon 13 to 14; Lane 13: exon 15 to 16; Lane 14: exon 17 to 18; Lane 15: exon 19;  
909 Lane 16: exon 20; Lane 17: exon 21; Lane 18: exon 22; Lane 19: exon 23; Lane 20: exon  
910 24; Lane 21: exon 25; Lane 22-23: exon 26.

911  
912 **Fig. 2.** Expression of human dipeptidyl peptidase 4 (hDPP4) in tissues from humans and  
913 mice. Tg2, hDPP4<sup>+/+</sup> transgenic mouse line 2; non-Tg, hDPP4<sup>-/-</sup> mouse. (A) Western blot

914 analysis of homogenized human and mouse tissues with an anti-hDPP4 polyclonal antibody  
915 or an anti- $\beta$ -actin polyclonal antibody (internal control). Arrows indicate the positions of  
916 hDPP4 (110 kDa). (B) Immunohistochemical analysis of hDPP4 expression in human, Tg2,  
917 and non-Tg mice tissues stained with an anti-hDPP4 polyclonal antibody. Sections were  
918 counterstained with hematoxylin. Scale bars, 50  $\mu$ m for large images of liver, kidney, small  
919 intestine, pancreas, spleen, and lymph node; and 20  $\mu$ m for large images of lung and brain;  
920 insets, 25  $\mu$ m.

921

922 **Fig. 3.** Innate immune responses in Tg2, non-Tg, and C57BL/6 mice. C57BL/6, non-Tg,  
923 and Tg2 mice received an intranasal inoculation of poly(I:C) or saline and were sacrificed  
924 24 h later (n = 4/group). Expression of pro-inflammatory cytokines and chemokines in  
925 saline- and poly(I:C)-inoculated animals. P-values were calculated using one-way ANOVA,  
926 followed by Tukey's post-test; ns: not significant; \*P < 0.05. Error bars indicate the  
927 standard deviation.

928

929 **Fig. 4.** Permissiveness of transgenic mice to infection by MERS-CoV. (A) The body  
930 weight of 10-week-old mice was monitored daily after intranasal inoculation of  
931 MERS-CoV at a dose of  $10^5$  TCID<sub>50</sub> (n = 8 for hDPP4-transgenic mouse line 2 (Tg2), n =  
932 10 for C57BL/6 mice). Error bars represent the standard deviation. \*\*P < 0.01, \*\*\*P < 0.001  
933 (two-way ANOVA). (B) Seroconversion of Tg2 mice inoculated with MERS-CoV. Titer of

934 MERS-CoV-specific neutralizing antibodies in mouse serum on Days 7, 14, and 35  
935 post-inoculation with MERS-CoV (Tg2, n = 3–5; C57BL/6, n = 4–6). The dotted line  
936 denotes the detection limit of the assay. Error bars represent the standard deviation. (C)  
937 Viral load in the respiratory tract of mice inoculated with MERS-CoV. NW, nasal wash  
938 fluid; Maxilla, maxilla including nostril; LW, lung wash fluid. Mice were euthanized at the  
939 indicated times post-viral inoculation (n = 3–4 per time point). Viral titer was expressed as  
940 the mean  $\pm$  standard deviation. The dotted line denotes the detection limit of the assay. \*\*P  
941 < 0.01, \*\*\*P < 0.001 (two-way ANOVA). (D) Quantitative real-time RT-PCR analysis of  
942 MERS-CoV viral RNA in splenocytes isolated from Tg2 and C57BL/6 mice. RNA was  
943 extracted from splenocytes infected with MERS-CoV at a multiplicity of infection of 1.  
944 RNA levels were normalized against  $\beta$ -actin (endogenous control).

945

946 **Fig. 5.** Histopathological changes in the lungs of human dipeptidyl peptidase 4  
947 (hDPP4)-transgenic mice inoculated with MERS-CoV. Representative images of lungs  
948 from hDPP4<sup>+/+</sup> transgenic mouse line 2 on Days 1, 3, 5, 7, 14, and 35 post-inoculation (p.i.).  
949 Mild but progressive interstitial infiltration was seen within 7 days p.i. (left column). IHC  
950 staining of sequential sections revealed abundant MERS-CoV antigen-positive cells in  
951 affected areas (middle column). Severe inflammation, with many mononuclear cells in the  
952 alveolar spaces and regenerated type II pneumocytes in the alveolar wall, was observed  
953 within 7 days p.i. (right column). Scale bars: left and middle columns, 100  $\mu$ m; right

954 column, 50  $\mu\text{m}$ ; insets of middle column, 20  $\mu\text{m}$ . HE, hematoxylin and eosin staining; IHC,  
955 immunohistochemistry using an anti-MERS-CoV nucleocapsid protein polyclonal antibody.  
956

957 **Fig. 6.** Double immunofluorescence images taken at 1 day p.i. showing human dipeptidyl  
958 peptidase 4 (hDPP4) (green) and MERS-CoV antigen (red) in the lungs of Tg2 mice  
959 infected with MERS-CoV. Viral antigen-positive cells in the lungs were hDPP4-positive  
960 bronchiolar epithelial cells (upper panels) and alveolar epithelial cells (lower panels).  
961 Original magnification,  $\times 600$ .

962

963 **Fig. 7.** Histopathological changes in the brain of human dipeptidyl peptidase 4  
964 (hDPP4)-transgenic mice inoculated with MERS-CoV. A, D, G show sagittal sections of the  
965 head, including the nasal cavity, olfactory bulb, and brain, of a Tg2 mouse infected with  
966 MERS-CoV (images taken at 3, 7, and 35 days p.i.). Right panels show the brain cortex  
967 from A, D, and G, respectively (B, E, F: hematoxylin and eosin staining; C, F, I:  
968 immunohistochemical analysis of MERS-CoV antigen). Neither lesions nor MERS-CoV  
969 antigen-positive cells were detected in the brain. Scale bars in A, D, G = 1 mm; scale bars  
970 in B, C, E, F, H, and I = 20  $\mu\text{m}$ .

971

972 **Fig. 8.** Susceptibility of adult human dipeptidyl peptidase 4 (hDPP4)-transgenic mice to  
973 MERS-CoV infection. Tg2, hDPP4<sup>+/+</sup> transgenic mouse line 2; non-Tg, hDPP4<sup>-/-</sup> mouse.

974 (A) The body weight of 25-week-old mice was monitored daily after intranasal inoculation  
975 with MERS-CoV (n = 6 Tg2 mice; and n = 7 non-Tg mice). \*P < 0.05 and \*\*\*P < 0.001  
976 (two-way ANOVA). (B) Seroconversion of Tg2 mice inoculated with MERS-CoV. Titer of  
977 MERS-CoV-specific neutralizing antibodies in mouse serum on Days 7, 14, and 35  
978 post-inoculation with MERS-CoV (Tg2, n = 4–6; non-Tg, n = 4). The dotted line denotes  
979 the detection limit of the assay. Error bars represent the standard deviation. (C) Viral titer in  
980 nasal wash fluid (NW), maxilla (including nostril), lung wash fluid (LW), and lungs of  
981 25-week-old Tg2 and non-Tg mice at 3 days post-inoculation (p.i.) (n = 4 mice per group).  
982 Viral titer is expressed as the mean ± standard deviation. The dotted line denotes the  
983 detection limit of the assay. \*\*P < 0.01 and \*\*\*P < 0.001 (two-way ANOVA).

984  
985 **Fig. 9.** Histopathological changes in the lungs of human dipeptidyl peptidase 4  
986 (hDPP4)-transgenic mice inoculated with MERS-CoV. Representative histopathological  
987 images of the lungs from 25-week-old Tg2 mice at 1, 3, 5, 7, 14, and 35 days  
988 post-MERS-CoV infection. Time-dependent recruitment of inflammatory cells to the lung  
989 (left and right columns). Marked inflammatory cell infiltration was noted at 7 days  
990 post-inoculation (p.i.) (J and L). Middle column, immunohistochemical staining for  
991 MERS-CoV antigen. Scale bars: left and middle columns = 100 µm; right column = 50 µm;  
992 insets of middle column = 20 µm. HE, hematoxylin and eosin staining; IHC,  
993 immunohistochemistry using an anti-MERS-CoV nucleocapsid protein polyclonal antibody.

994

995 **Fig. 10.** Identification of cells infiltrating the lung of Tg2 mice infected with MERS-CoV.

996 Representative images of lungs from 10-week-old (Young) and 25-week-old (Adult)

997 hDPP4<sup>+/+</sup> transgenic mice (line 2) on Day 7 post-inoculation (p.i.). Infiltrating cells were

998 positive for Iba-1 (green) or CD3 (brown). Bars, 20  $\mu$ m. Upper panels: hematoxylin and

999 eosin staining (HE); Middle and lower panels: immunohistochemistry (IHC) using an

1000 anti-Iba-1 polyclonal antibody and an anti-CD3 monoclonal antibody.

1001

1002 **Fig. 11.** Cytokine and chemokine levels and expression of type I interferon (IFN) genes in

1003 the lungs of Tg2 mice infected with MERS-CoV. Cytokine and chemokine levels in lung

1004 samples from 10-week-old (A) and 25-week-old (B) mice. Tg2 mice were inoculated with

1005 MERS-CoV or cell culture medium containing 2% FBS. Lungs were collected at the

1006 indicated times post-viral inoculation (n = 3–4 mice per time point). Data represent the

1007 mean  $\pm$  standard deviation. The dotted line denotes the detection limit of the assay. \*P <

1008 0.05, \*\*P < 0.01, and \*\*\*P < 0.001 (two-way ANOVA). (C) Quantitative real-time RT-PCR

1009 analysis of type I IFN gene expression in lung homogenates from Tg2 mice inoculated with

1010 MERS-CoV or cell culture medium containing 2% FBS. RNA levels were normalized

1011 against  $\beta$ -actin (endogenous control). Data represent the mean  $\pm$  standard deviation. The

1012 dotted line denotes the detection limit of the assay. \*P < 0.05 and \*\*\*P < 0.001 (two-way

1013 ANOVA).

1014 **Table 1.** Primers used for PCR of human DPP4 exons

Target	Size (bp)	Sequence (5'→3')	
		Forward	Reverse
Exon 1	130	AATGTTTAACTCGGGCCGA	CGGAAGTGAGCGTTCAGAGA
Exon 2	162	GGACTTGATCTGCTCGGCTT	CCTGACCTGAGCTCCAAGT
Exon 3	391	ACACACACTCTCACACT	TTCAGTGCCATAAAAGCCCA
Exon 4	468	GTGCAAAGGGAGAAAGACTGA	CCACTTTGCCATATGCTGCA
Exon 5	562	GTGCACAGTGATGGCAATGA	CCACCATGCCCGACTTTAAC
Exon 6-7	330	GTCTCTATAGTGAGTGGCCA	TCTGACAACTGGAGAGACTCAC
Exon 8	565	GGTCAGCCTTCTCGGTCTTC	GGAGACATCTGGTGCTGTGA
Exon 9	440	AGCCCAGCAAATGCAAAGTG	GCCAGATGCTGTTGACTTCAG
Exon 10	296	TGCAGACGTTTTTGTGCAGT	GGCTGTGATCCACTTTGCCA
Exon 11	274	CCAAGGTCTGGCAATAGTCA	TTCCTCTCCCAACTGCAC
Exon 12	299	GAGCTTCCAGAAGGACCCAG	GCTGACTCATCCATAAAACCCC
Exon 13-14	848	TGCTTGCAGCCAGAAGTCAT	CTTCTGGGCAAAGAGGGCAT
Exon 15-16	708	CTCCGTGCACACTTAGGCTT	GGAGCTGCTTCGAAGTGAGT

Exon 17–18	847	GCCCTGTGCCTTTCCAGTAA	GCATGTTCTCCAAATCCCTTCC
Exon 19	247	TGCTACTGACGGACATGAGG	GAAAGGACGCATTGGCTCC
Exon 20	549	GGATGCATACTTCTCCACGG	AGGACATATGCCAACTCCCT
Exon 21	281	GCAGAGAACAAATGGCAGGG	ACTGCCCAGAGACCTAAGACT
Exon 22	206	AATGTGGAAACTGCGACTCG	TCTCTTTGTACCTGGCAGCA
Exon 23	567	AGGTGCTTAGCCACCCTTT	GAGAGTCTTCTGGGCTCTAAAGG
Exon 24	364	TCCCTTCCAGTCTGTCTCC	CAGTCTTGCCCTCATGCTT
Exon 25	239	CTTCCCACCCCTTGGTACC	CCTGTCTGTGGCACTGCTAA
Exon 26 (1)	784	TAGACCCCTCTTTGACCCC	GAACAGCTTCTCCGAGGG
Exon 26 (2)	723	AAGGGATGGCAAGATGTGGG	TCCATATGCCAGTGCGGTTT

1015

1016

1017

1018

1019

1020

1021 **Table 2.** Virus isolation, detection of viral antigens by immunohistochemistry, and detection of the MERS-CoV genome by real-time  
 1022 PCR in tissues from Tg2 and non-Tg mice inoculated with MERS-CoV

Animal	Liver			Spleen			Kidney			Heart			Lung			Intestine			Brain			Blood			
	I	A	G	I	A	G	I	A	G	I	A	G	I	A	G	I	A	G	I	A	G	I <sup>1</sup>	A	G	
Tg2	-	-	NE	-	-	-	-	-	-	-	-	NE	+	+	NE	-	-	NE	-	-	-	-	-	+	
Non-Tg	-	-	NE	-	-	-	-	-	-	-	-	NE	-	-	NE	-	-	NE	-	-	-	-	-	-	-

1023 I: virus isolated; A: viral antigens; G: viral genome.

1024 +: virus was isolated, or viral antigens or the viral genome was detected, in tissues.

1025 -: no virus, antigen, or genome was detected in tissues.

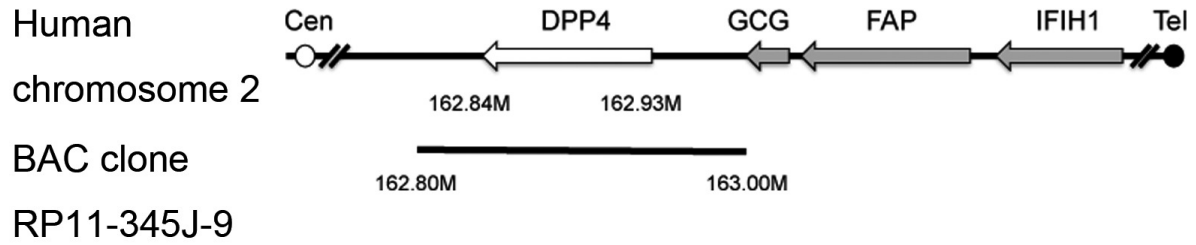
1026 Tg2 = hDPP4<sup>+/+</sup> transgenic mouse line 2; non-Tg = hDPP4<sup>-/-</sup> mouse.

1027 NE: not examined.

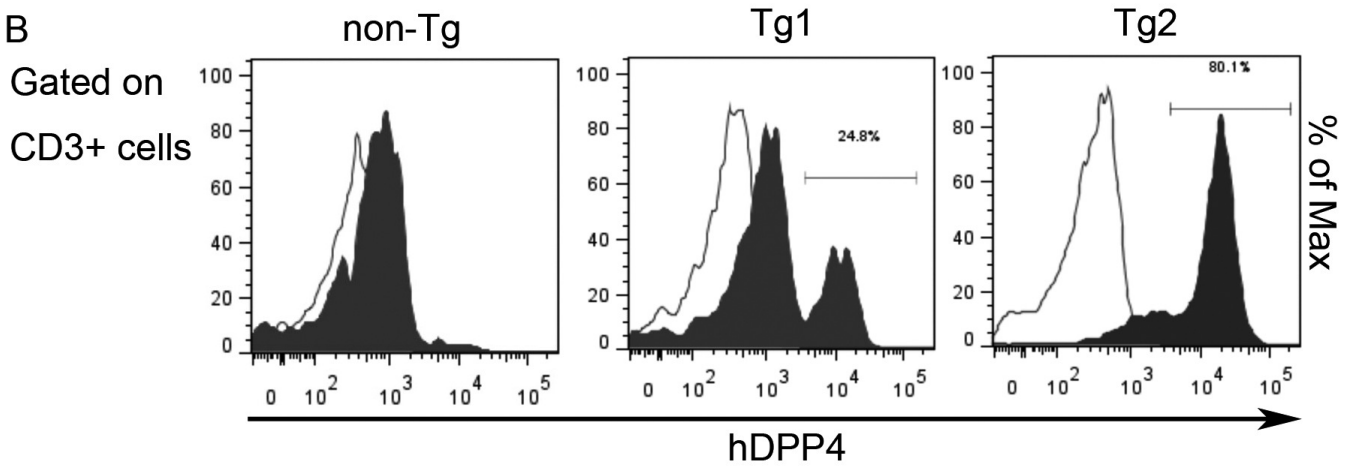
1028 <sup>1</sup>: serum samples used for analysis.

1029 <sup>2</sup>: viral genome was detected in samples at 3 and 5 days p.i.

A



B



C

